Geophysical Journal International

Geophys. J. Int. (2012) **190,** 1625–1639 doi: 10.1111/j.1365-246X.2012.05560.x

GPS and seismic constraints on the $M = 7.3$ 2009 Swan Islands earthquake: implications for stress changes along the Motagua fault and other nearby faults

Shannon E. Graham,[1] Charles DeMets,[1] Heather R. DeShon,[2] Robert Rogers,[3] Manuel Rodriguez Maradiaga,[4] Wilfried Strauch,[5] Klaus Wiese[4] and Douglas Hernandez[6]

[1] *Department of Geoscience, University of Wisconsin-Madison, Madison,* WI 53706, *USA. E-mail: segraham@wisc.edu*
[2] *Center for Earthquake Research and Information, University of Memphis, Memphis, Tennessee, USA*
[3] *Department of Geology, California State University Stanislaus, Turlock,* CA 95382, *USA*
[4] *Instituto Hondureño de Ciencias de la Tierra,Universidad Nacional Autonoma de Honduras Tegucigalpa, Honduras*
[5] *Observatorio Sismico del Occidente de Panamá*
[6] *Servicio Nacional de Estudios Territoriales, Ministerio de Medio Ambiente y Recursos Naturales, Km.* 5 1/2 *carretera a Santa Tecla, Colonia y Calle Las Mercedes, Plantel ISTA, San Salvador, El Salvador*

Accepted 2012 May 29. Received 2012 May 16; in original form 2011 November 14

SUMMARY

We use measurements at 35 GPS stations in northern Central America and 25 seismometers at teleseismic distances to estimate the distribution of slip, source time function and Coulomb stress changes of the $M_w = 7.3$ 2009 May 28, Swan Islands fault earthquake. This event, the largest in the region for several decades, ruptured the offshore continuation of the seismically hazardous Motagua fault of Guatemala, the site of the destructive $M_s = 7.5$ earthquake in 1976. Measured GPS offsets range from 308 millimetres at a campaign site in northern Honduras to 6 millimetres at five continuous sites in El Salvador. Separate inversions of geodetic and seismic data both indicate that up to ∼1 m of coseismic slip occurred along a ∼250-km-long rupture zone between the island of Roatan and the eastern limit of the 1976 $M = 7.5$ Motagua fault earthquake in Guatemala. Evidence for slip ∼250 km west of the epicentre is corroborated independently by aftershocks recorded by a local seismic network and by the high concentration of damage to structures in areas of northern Honduras adjacent to the western limit of the rupture zone. Coulomb stresses determined from the coseismic slip distribution resolve a maximum of 1 bar of stress transferred to the seismically hazardous Motagua fault and further indicate unclamping of normal faults along the northern shore of Honduras, where two $M > 5$ normal-faulting earthquakes and numerous small earthquakes were triggered by the main shock.

Key words: Space geodetic surveys; Seismic cycle; Earthquake dynamics.

1 INTRODUCTION

West of the Mid-Cayman spreading centre (Fig. 1), the 750 km long, submarine Swan Islands fault and its onshore continuation, the Motagua–Polochic fault zone of Guatemala carry most of the motion between the Caribbean and North America plates. Large destructive earthquakes along these faults, including the 1976 February 4 $M_s = 7.5$ Motagua fault earthquake, which caused 100 000 casualties in Guatemala (Plafker 1976), and the 1816 July 22, $M_w \sim 7.5$ Polochic fault earthquake (White 1985) call for a better understanding of their interseismic strain accumulation (Lyon-Caen *et al*. 2006) and tectonic roles within the complexly deforming western end of the Caribbean Plate (Guzman-Speziale *et al*. 1989; Guzman-Speziale 2001; Rogers & Mann 2007; Alvarez-Gomez *et al*. 2008; Rodriguez *et al*. 2009).

The focus of this study is the most recent large earthquake along the Swan Islands/Motagua–Polochic fault system, the $M_w = 7.3$ 2009 May 28 earthquake on the Swan Islands fault near Roatan island off the north coast of Honduras (Fig. 1). This earthquake not only caused seven deaths and extensive damage in northern Honduras, but appears to have triggered numerous other smaller earthquakes ∼50–100 km from the rupture zone (Fig. 2b). Here, we present a combined GPS and seismic study of the 2009 May 28 Swan Islands fault earthquake, with a focus on the following: (1) the magnitude and spatial distribution of coseismic slip during the 2009 main shock and their relationship to the 1976 Motagua

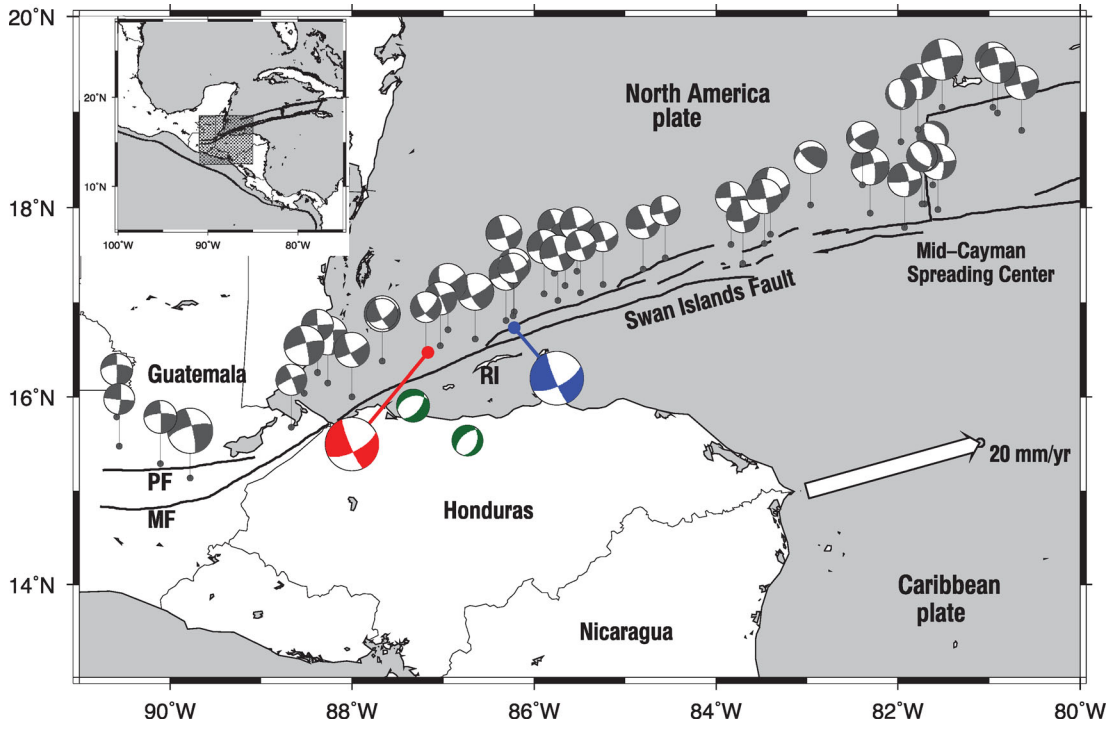

Figure 1. Tectonic setting of the study area. White arrow denotes motion of the Caribbean Plate relative to North America Plate predicted by MORVEL (DeMets *et al*. 2010). Black focal mechanisms are from the global CMT catalogue spanning 1976 January through 2011 June. Red and blue focal mechanisms depict the global CMT and NEIC estimates of the 2009 May 28 earthquake epicentre, respectively. Green focal mechanisms (from the Global CMT Catalogue) are for the $M = 5.1$ 2009 June 2 and $M = 5.4$ 2009 June 8 normal-faulting earthquakes described in the text and are positioned at the location given by our local seismic network. Motagua fault location from Plafker (1976). Swan Islands fault location from Rogers & Mann (2007) and Mann *et al*. (1991). MF, Motagua fault; PF, Polochic fault; RI, Roatan Island.

fault rupture zone, (2) the distribution of Coulomb stress changes along the nearby Motagua–Polochic fault system and normal faults in northern Honduras and (3) the seismic hazard implications of our results. We accomplish the first of these via elastic half-space modelling of GPS offsets recorded within 300 km of the rupture and an inversion of waveforms from 25 seismometers at teleseismic distances. We then use Coulomb stress changes determined from the best-fitting geodetic fault-slip distribution to interpret two $M > 5$ normal-faulting earthquakes in northern Honduras that occurred 5 and 11 d after the main shock and numerous locally recorded earthquakes associated with these possibly triggered events.

2 FAULT-SLIP ESTIMATE FROM GPS

2.1 GPS network and observations

The 2009 May 28 earthquake caused measurable offsets at 7 continuous and 28 campaign GPS sites in Honduras and El Salvador within several hundred kilometres of the epicentre (Figs 2b and 3; Table 1). Campaign measurements in Honduras consist of several multiday occupations of each site between mid-2000 and mid-2007 before the 2009 May 28 earthquake and one or two 48 h or longer occupations after the earthquake. The campaign sites closest to the rupture (FRT1, LCEB, MEZA) were occupied 1–3 weeks after the earthquake; other campaign stations were occupied 9 months or longer after the earthquake (Table 1). Rodriguez *et al*. (2009) describe and show many of the Honduran station time series prior to the earthquake. Data from all but one of these stations are available from the UNAVCO data archive; data for continuous site SSIA are available from the NOAA CORS archive.

All the GPS data used for this study were processed with Release 6.1 of the GIPSY software suite from the Jet Propulsion Laboratory (JPL). No-fiducial daily GPS station coordinates were estimated using a precise point-positioning strategy (Zumberge *et al*. 1997), including constraints on *a priori* tropospheric hydrostatic and wet delays from Vienna Mapping Function (VMF1) parameters (http://ggosatm.hg.tuwien.ac.at), elevation dependent and azimuthally dependent GPS and satellite antenna phase centre corrections from IGS08 ANTEX files (available via ftp from sideshow.jpl.nasa.gov), and corrections for ocean tidal loading from the TPX0.7.2 ocean tide model (http://froste.oso.chalmers.se). Wide- and narrow-lane-phase ambiguities were resolved for all the data using GIPSY's single-station ambiguity resolution feature.

All daily no-fiducial station location estimates were transformed to ITRF2008 (Altamimi *et al*. 2011) using daily seven-parameter Helmert transformations from JPL. Spatially correlated noise between stations is estimated from the coordinate time-series of well-behaved continuous stations from within and outside the study area and is removed from the time-series of all sites (Marquez-Azua & DeMets 2003). The coseismic offsets at our campaign sites (Table 1, Fig. 3) are calculated by estimating a single best-fitting slope, a step offset on the day of the earthquake and an intercept from all the observations preceding the earthquake and the first site occupation afterwards. Offsets at the seven continuous stations are calculated from the difference in the weighted average station locations for the 5 d immediately before and after the earthquake. Although we estimated and used the vertical coseismic offsets in the early stages

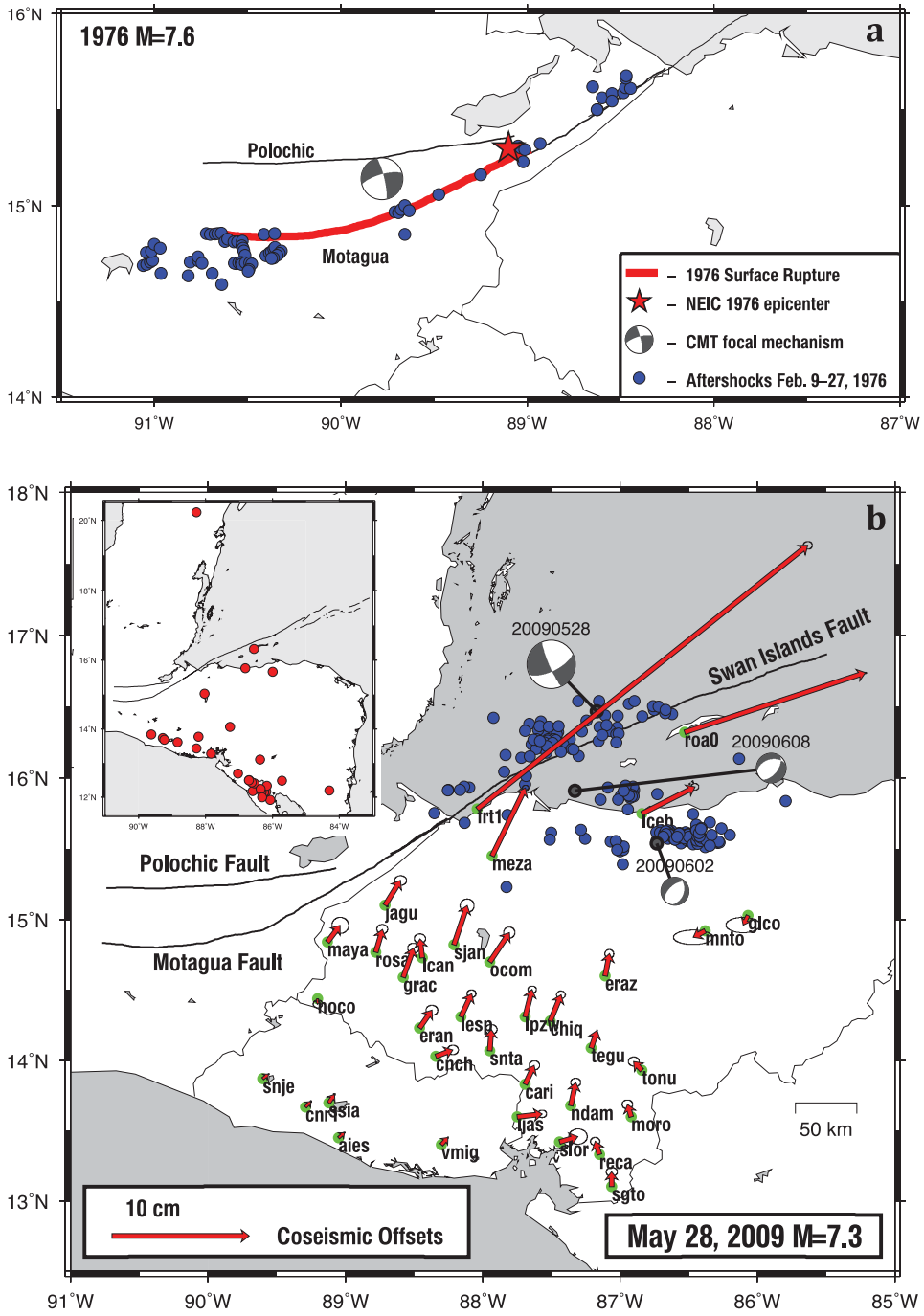

Figure 2. (a) Surface rupture (after Plafker 1976) and aftershocks (after Langer & Bollinger 1979) from the 1976 ($M_s = 7.5$) Motagua fault earthquake. Red star denotes the NEIC earthquake epicentre. (b) Observed coseismic offsets (red arrows) and 2-D, 1-σ offset uncertainties for the 2009 ($M_w = 7.3$) Swan Islands fault earthquake. Focal mechanisms are for the 2009 May 28, 2009 June 2 and 2009 June 8 earthquakes and are from the global CMT catalogue. Blue circles indicate aftershocks observed by a portable seismic array (see text). (Inset) Red circles denote station locations for the local seismic network and permanent stations used in determining the aftershock locations.

of modelling, the inversion results were insensitive to them due to their high uncertainties. Hereafter, we employ only the horizontal offsets to estimate the coseismic fault-slip.

Fig. 2(b) shows the estimated coseismic offsets. The largest measured offsets were at sites FRT1 (308 ± 3 mm), ROA0 (138 ± 0.7 mm), MEZA (55 ± 3 mm) and LCEB (43 ± 3 mm), all located relatively near the offshore rupture zone. As expected, the coseismic offsets decrease with increasing distance from the fault and, for most sites, agree with the pattern of deformation anticipated for a left-lateral strike-slip fault. Small but systematic northeastward offsets of 6 ± 1 mm were recorded at all five continuous stations in El Salvador, 350 km from the rupture zone. Continuous measurements at station ROA0 near the epicentre indicate that cumulative postseismic transient slip was no more than 5 per cent of the coseismic

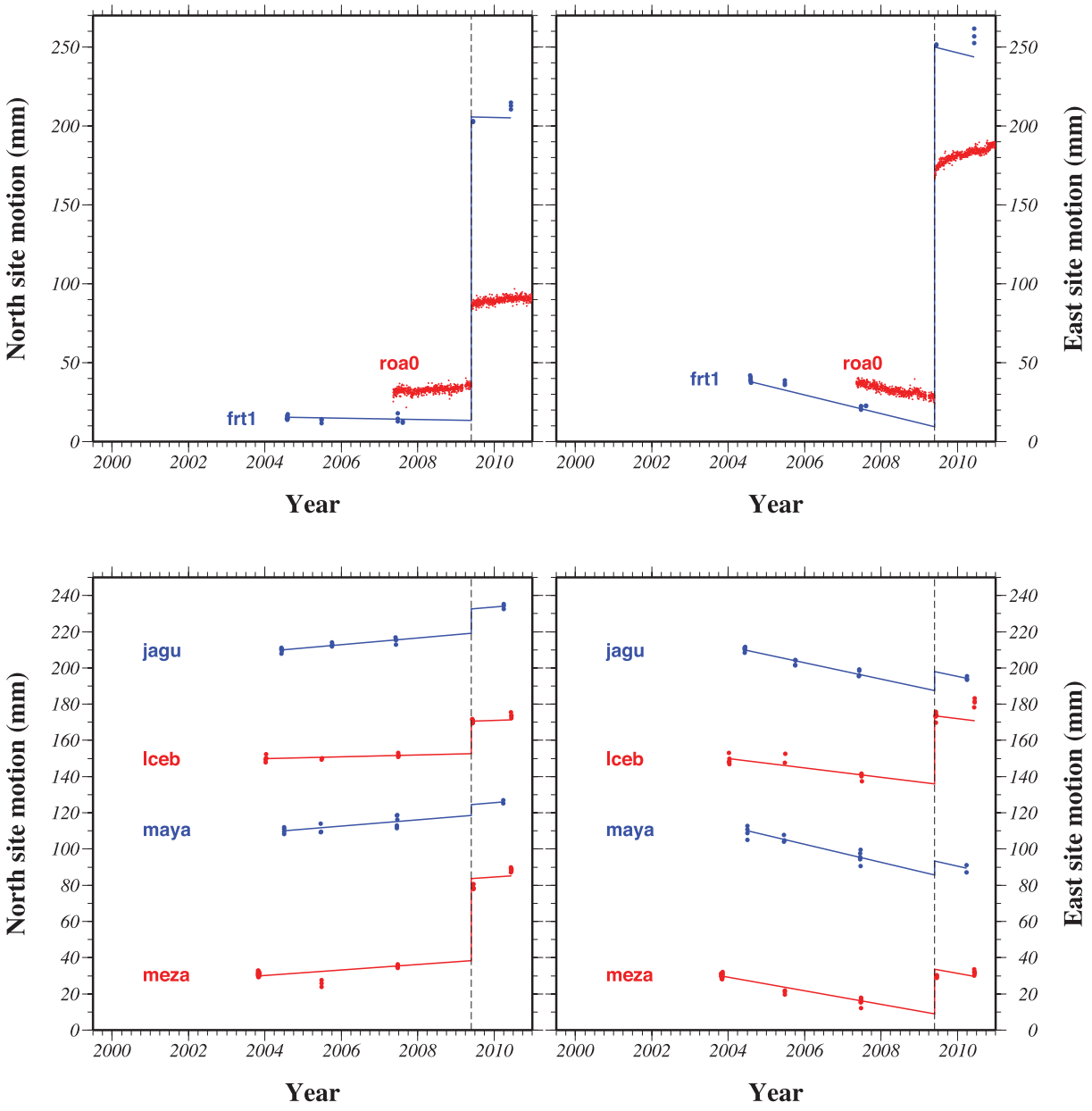

Figure 3. Time series for GPS sites with coseismic offsets that are used to define the best-fitting coseismic slip distribution shown in later figures. Dashed vertical line indicates time of earthquake.

offset during the several week-long period between the earthquake and our first reoccupation of our campaign sites. We thus ignore the influence of post-seismic slip in our estimate of the coseismic slip distribution. As a further means of estimating the coseismic slip free from the influence of any post-seismic afterslip, we also invert teleseismic waveforms (Section 3).

2.2 Temporary seismic network

Aftershocks of the May 28 $M = 7.3$ main shock were recorded by four temporarily deployed seismometers in northern Honduras (installed by coauthor Wilfried Strauch) and three permanent seismometers in Mexico, El Salvador and Nicaragua (Fig. 2b inset). Other regional permanent stations were used for larger events or if needed to better locate a particular aftershock (Fig. 2b inset). Two of the temporary stations were installed on June 1 and 3 and the remaining two on June 26 and 30. A total of 216 aftershocks were observed from June through August, when most activity had ceased. Locations, determined from *P*- and *S*-wave arrivals, are distributed along a 250-km-long segment of the Swan Islands fault between Roatan and the Guatemalan coast and along normal faults both in northern Honduras and offshore (Fig. 2b). Events were detected and recorded with EARTHWORM and preliminary data processing (phase picking, location and magnitude) was done with SEISAN by the seismologist on duty at INETER, Managua. W. Strauch completed the final data processing with the inclusion of regional stations if needed, removal of poor phase picks and application of frequency filters for improved phase picking. Due to the scarcity of stations and non-optimal geometry, the

Table 1. Coseismic offsets estimated from GPS observations described in text. Offsets for sites marked by asterisks were used to estimate the best-fitting geodetic slip distribution. Final column indicates the number of days that lapsed between the 2009 May 28 earthquake and the first post-seismic occupation of the GPS site. C denotes continuous station.

			Observed coseismic offset (mm)				
Site ID	Longitude	Latitude	East	1σ	North	1σ	Days between EQ and observation
ROA0*	273.47	16.32	131.4	0.6	43.4	0.3	C
FRT1*	271.96	15.78	240.66	2	192.13	2	18
JAGU*	271.29	15.1	11.21	3	18.16	2	309
LCEB*	273.16	15.75	38.56	2	19.46	2	9
MAYA*	270.87	14.84	9.32	4	12.23	4	307
MEZA*	272.07	15.45	24.19	1.5	49.54	1	20
AIES	270.95	13.45	4.3	0.3	3.8	0.2	C
CNR1	270.71	13.67	4	0.4	4	0.3	C
SNJE	270.4	13.87	4.3	0.3	3.4	0.2	C
SSIA	270.88	13.7	4.1	0.5	6.1	0.4	C
VMIG	271.7	13.4	4.7	0.3	5.2	0.3	C
CARI	272.31	13.83	6.61	3	13.89	2	393
CHIQ	272.49	14.28	7.95	2	19.18	2	370
CNCH	271.66	14.03	12.29	3	4.67	2	372
ERAN	271.54	14.23	9.03	3	13.01	2	371
ERAZ	272.89	14.6	3.15	2	16.17	2	392
GLCO	273.93	15.03	−3.49	8	−7.04	4	386
GRAC	271.42	14.59	7.54	3	21.33	2	374
LCAN	271.56	14.73	−1.71	3	13.88	2	375
LESP	271.84	14.31	7.88	2	16.89	2	371
LJAS	272.25	13.6	18.27	2	2.07	2	389
LPZW	272.31	14.31	5.02	2	19.94	2	371
MNTO	273.62	14.92	−8.79	10	−4.67	3	387
MORO	273.08	13.6	−2.66	3	9.01	2	388
NDAM	272.64	13.68	3.65	2	16.77	2	386
NOCO	270.8	14.44	−0.05	2	−3.9	2	375
OCOM	272.05	14.7	14.33	3	21.39	3	380
RECA	272.85	13.33	−3.14	2	9.63	2	389
ROSA	271.22	14.77	4.9	3	16.67	2	378
SGTO	272.94	13.1	−0.04	3	10.88	2	388
SJAN	271.79	14.82	9.67	3	28.61	3	380
SLOR	272.56	13.42	13.42	4	3.93	4	386
SNTA	272.05	14.07	1.13	3	15.46	2	371
TEG1	272.79	14.09	4.33	0	12.86	0	C
TONU	273.16	13.93	−6.05	3	6.43	2	383

horizontal location uncertainty for the aftershock locations is on average 5–10 km.

2.3 Inverse modelling of the GPS site offsets: methods, validation and results

We estimate the distribution and magnitude of coseismic slip along the Swan Islands fault via an inversion of the coseismic offsets subject to two constraints: smoothing is used to prevent solutions that are unrealistically complex and a non-negativity constraint is used to require left-lateral slip at all locations on the fault. We solve a version of the linear system $\mathbf{Gm} = \mathbf{d}$ that employs weighting based on uncertainties in the coseismic offsets and a smoothing parameter, as follows

$$\begin{bmatrix} \mathbf{WG} \\ \alpha\mathbf{F} \end{bmatrix} \mathbf{m} = \begin{bmatrix} \mathbf{Wd} \\ 0 \end{bmatrix}, \quad (1)$$

where $\mathbf{d}$ is a data vector comprised of the north and east displacements at each GPS site, $\mathbf{m}$ is the best slip values at all the fault nodes, $\mathbf{G}$ is a Green's function matrix that specifies how the surface responds to assumed unit slip across a particular patch of the fault, $\mathbf{W}$ is a square diagonal weighting matrix composed of the reciprocal of the offset uncertainties, α is the chosen smoothing coefficient and $\mathbf{F}$ is a smoothing matrix (Correa-Mora *et al*. 2008). The Green's function matrix ($\mathbf{G}$) has dimensions $2n \times m$, with n equal to the number of GPS stations used in the inversion and m equal to the number of rectangular patches used to represent the fault. Both the smoothing coefficient and matrix (α and $\mathbf{F}$, respectively) are treated as pseudo-data.

Forward modelling of surface deformation to generate the entries of the $\mathbf{G}$ matrix is accomplished with DISL, a code for elastic half-space dislocation modelling (Larsen 1992). Motion across the fault is constrained to be purely strike-slip, a reasonable approximation since the vertical coseismic displacement recorded at continuous station ROA0 near the rupture zone (6 ± 1 mm) was only a few percent of the horizontal coseismic movement (138 ± 0.7 mm). Displacements at the location of the GPS sites are calculated by bilinear interpolation from the elastic displacements from the nearest neighbour surface nodes. To approximate the strike and location of the Swan Islands fault, we divide the fault into six patches of constant down-dip width (0–15 km) (Fig. 4) with the fault location given by

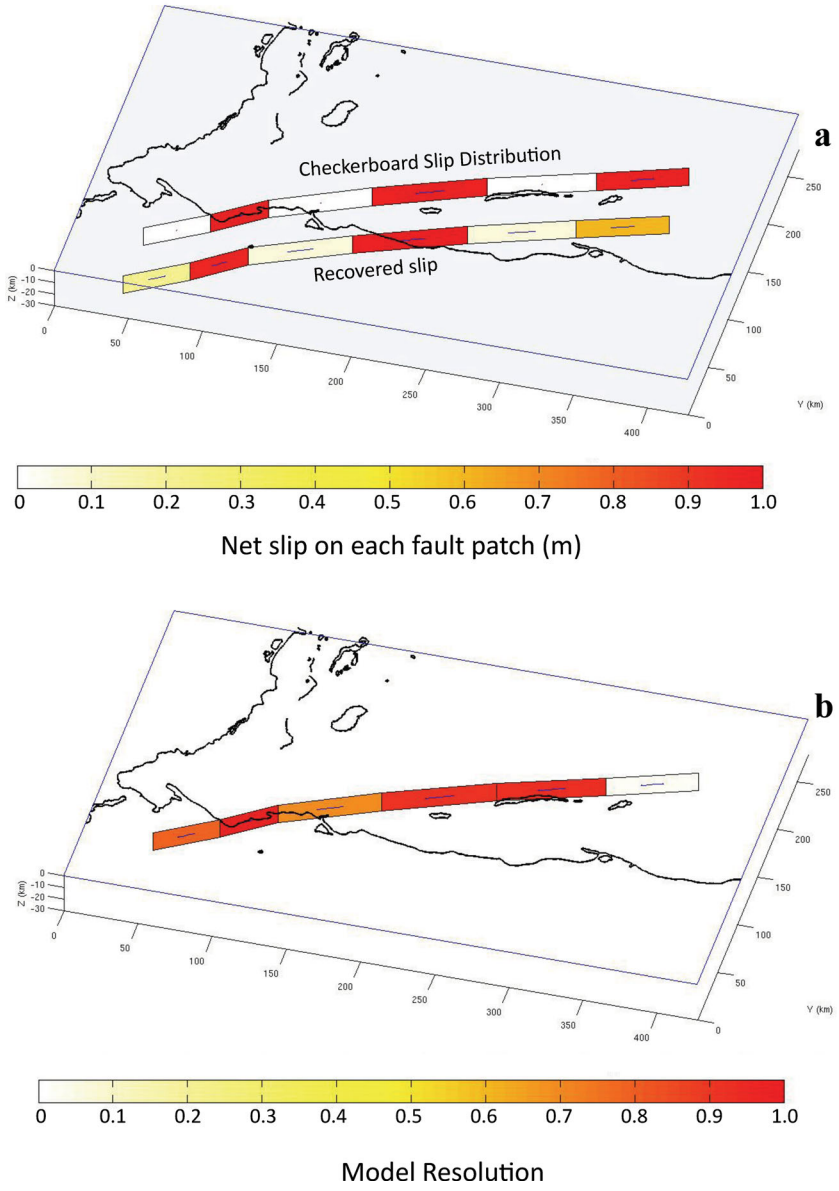

Figure 4. (a) Test of resolution and ability to recover a known slip distribution (top) from noisy synthetic data with the six GPS stations that were used to estimate the geodetic fault-slip distribution. The slip model recovered from the data, which is shown immediately beneath the checkerboard (known) distribution, matches within 10 per cent the starting values for the central four fault patches. Slip is recovered more poorly for the eastern- and westernmost patches, which have lower model resolution. (b) Model resolution calculated from (2). The model resolution depends on the GPS site distribution relative to the modelled fault location and the smoothing coefficient used for the checkerboard inversion. Slip is most poorly resolved for the easternmost fault patch, which is the most distant from the GPS network.

the SeaMARC II survey of the Swan Islands fault (Rosencrantz & Mann 1991; Rogers & Mann 2007). The length of Swan Islands fault used in the inversion was determined from the distribution of aftershocks (Fig. 2b). Discretizing the fault into 12 patches along strike with either one or two layers down-dip did not significantly alter the fit to the data or the distribution of slip along the fault. We thus opted for the simpler fault discretization.

The inversion procedure disallows slip in the wrong direction using a non-negative least-squares algorithm (Lawson & Hanson 1974) that minimizes $\|\mathbf{Gm} - \mathbf{d}\|^2$ for all elements of m greater than zero. The resolution matrix $\mathbf{R}_\mathrm{m} = \mathbf{G}^\#\mathbf{G}$, where $\mathbf{G}^\# = (\mathbf{G}^T\mathbf{G} + \alpha^2\mathbf{F}^T\mathbf{F})^{-1}\mathbf{G}^T$, is used to determine how well resolved the slip solution is as a function of location on the fault. Data importances $\mathbf{R}_\mathrm{d} = \mathbf{G}\mathbf{G}^\#$ are used to determine the relative importances of the individual data to the inversion.

Best-fitting models from the inversion were determined by searching for the smoothing coefficient α and model vector $\mathbf{m}$ that minimize χ^2_ν, where χ^2_ν is defined as χ^2/dof and the degrees of freedom (dof) are given by

$$dof = trace\left(\mathbf{I} - \mathbf{G}\left(\mathbf{G}^T\mathbf{G} + \alpha^2\mathbf{F}^T\mathbf{F}\right)^{-1}\mathbf{G}^T\right) \quad (2)$$

(Hansen 1992). Minimizing χ^2_ν by varying the smoothing coefficient constitutes one rigorous approach to finding the optimal trade-off between the data least-squares fit and complexity of the best slip distribution. Although we also evaluated the L-curve method for

determining the optimal smoothing coefficient (Hansen 1992), it resulted in a poorer fit to the data. We thus use the χ^2_ν method.

2.4 Model validation via checkerboard test

To ascertain how well slip can be resolved across the offshore Swan Islands fault using offsets from the onland GPS network, we used DISL to predict synthetic displacements at each GPS site given a checkerboard pattern of alternating fault-slip patches of 0 and 1 m (Fig. 4a). Prior to their inversion, these synthetic displacements were perturbed by Gaussian noise assuming typical GPS uncertainties of ± 1, ± 2 mm for the north and east components, respectively. An inversion of the noisy synthetic data using (1) recovers the specified fault-slip values to better than 10 per cent for the central four fault patches. The initial slip values for both the eastern- and westernmost patches, where there are few or no GPS stations, were recovered only to the nearest 20 and 40 per cent, respectively (Fig. 4a). The formal model resolution, which indicates how well slip can be resolved as a function of location on the fault surface (Fig. 4b), supports the checkerboard results that slip on the fault west of Roatan Island is better resolved than slip east of Roatan. We chose the model with a smoothing coefficient of 0.03 to minimize χ^2_ν and produce a reliable model resolution.

2.5 Best-fitting fault-slip solution from GPS offsets

A preliminary inversion of all 35 coseismic offsets to determine the data importance for the offset at each site indicates that 91 per cent of the total data importance comes from the six sites nearest the rupture zone. Offsets at the remaining 29 sites thus contribute negligibly to the estimated fault-slip solution. We therefore opted to estimate the coseismic slip distribution from the offsets at the six sites nearest the rupture zone (Fig. 5a) and use the remaining 29 offsets to test the predictive power of the best-fitting slip solution.

Fig. 5a shows the best-fitting fault-slip values from our six-site inversion. Coseismic fault-slip ranges from 0.9 m near the west end of the rupture zone, offshore from site FRT1 (Fig. 5a), to 0.2–0.4 m near the west and east ends of the fault, respectively. Slip values average 0.7 m close to Roatan Island, as well as farther west where numerous aftershocks were recorded by the temporary seismic network. The western limit of coseismic slip in 2009 nearly reaches the eastern limit of the 1976 Motagua fault earthquake rupture (Fig. 6).

As part of our analysis, we examined the trade-off between the GPS model fit and assumed western limit of the 2009 earthquake rupture zone. The misfit increases rapidly as we omit segments at the western end of the Swan Islands fault (Fig. 7). In particular misfits for models that exclude the westernmost two patches are hundreds of times larger than the model in which the fault extends to intersect the onshore Motagua fault (the six-fault-patch model). All the solutions that omit the westernmost $\sim$75 km of the fault misfit the well determined coseismic offsets at sites FRT1 and MEZA in northern Honduras at many times their estimated uncertainties. We conclude that high slip along the Swan Islands fault directly offshore from site FRT1 is required and hereafter use the six-fault-patch model as our preferred geodetic solution. Adding segments west of the six-segment preferred model does not further improve the fit.

The best model fits the two largest offsets, 308 ± 4 mm at FRT1 and 138 ± 0.7 mm at ROA0, to within 4 mm and 0.03 mm, respectively, and has a RMS misfit for all six sites of 3.7 mm (χ^2_ν is 2.72). The coseismic offsets are therefore fit close to their estimated uncertainties, which we regard as successful given the simplifying approximations implicit in our model. The two largest misfits occur at sites JAGU and MAYA, (Fig. 5b). Because neither of these sites was occupied until 300 d after the earthquake, their measured offsets may be less reliable estimates of the coseismic motion.

The seismic moment estimated from the best-fitting slip solution is 12.4×10^{19} Nm ($M_w = 7.3$) assuming a shear modulus of 40 GPa. The geodetic moment agrees with seismologic moments of 11.0×10^{19} Nm from the USGS and 12.8×10^{19} Nm from the Global CMT catalogue, lending confidence in our solution.

2.6 Slip solution validation

To test our best-fitting slip solution, we used it as a forward model to predict coseismic offsets at the 29 low-importance GPS sites whose measured coseismic offsets were excluded from the determination of the best-fitting solution (Fig. 8). Encouragingly, offsets predicted by the forward model at the five stations in El Salvador where continuous observations strongly constrain the coseismic offsets (inset to Fig. 8) match the measured offset directions and magnitudes to within $\sim$2 mm. At the 24 campaign sites in Honduras, the best slip solution correctly predicts many of the measured offset directions, but underestimates the offset magnitudes at nearly all the stations (Fig. 8). We consider the offsets measured at these 24 sites to be less reliable because these sites were last occupied in mid-2007, roughly 2 yr before the earthquake. We tested whether the fits at these 29 sites could be improved via a simultaneous inversion of the offsets for all 35 GPS sites, but found negligible improvement in the fit because the slip solution is dominated by information from the six stations closest to the rupture zone (see Section 2.5).

The best-fitting slip solution reduces the variance of the 29 low-importance offsets by 86 per cent, indicating that the best-fitting solution successfully predicts the coseismic offsets at these sites. This gives us confidence in the reliability of the best-fitting coseismic slip distribution. In Section 3, we arrive at a similar conclusion from an inversion of seismic waveforms for the 2009 May 28 earthquake.

2.7 Slip solution uncertainties

Below, we assess the sensitivity of the estimated slip solution to our assumption of a vertical fault and the location we use for the Swan Islands fault. To determine the influence of our vertical dip assumption, we substituted faults that dip either 68° to the south, corresponding to the fault dip for the focal mechanism from the global CMT catalogue, or 68° to the north. For the former fault dip, re-inversion of the six offsets that were used to find the best-fitting solution reduces by 30 per cent the slip magnitude on the fault patch adjacent to site FRT1 of our best solution, but causes little change to the slip on the other fault patches. For the latter fault dip, the slip magnitude on the fault patches adjacent to sites FRT1 and ROA0 are increased by 40 and 20 per cent, respectively, while slip on the remaining resolvable patches change by no more than 10 per cent. Both dipping models were used as input for our Coulomb stress change calculations to ascertain their influence on our conclusions below. We found that all major features present with our best-fitting model remain the same.

To our knowledge, no definitive location for the Swan Islands fault where it comes onshore from the Caribbean Sea has been published. We therefore adopted a shortest-path location for the fault trace between the part of the Swan Islands fault mapped with

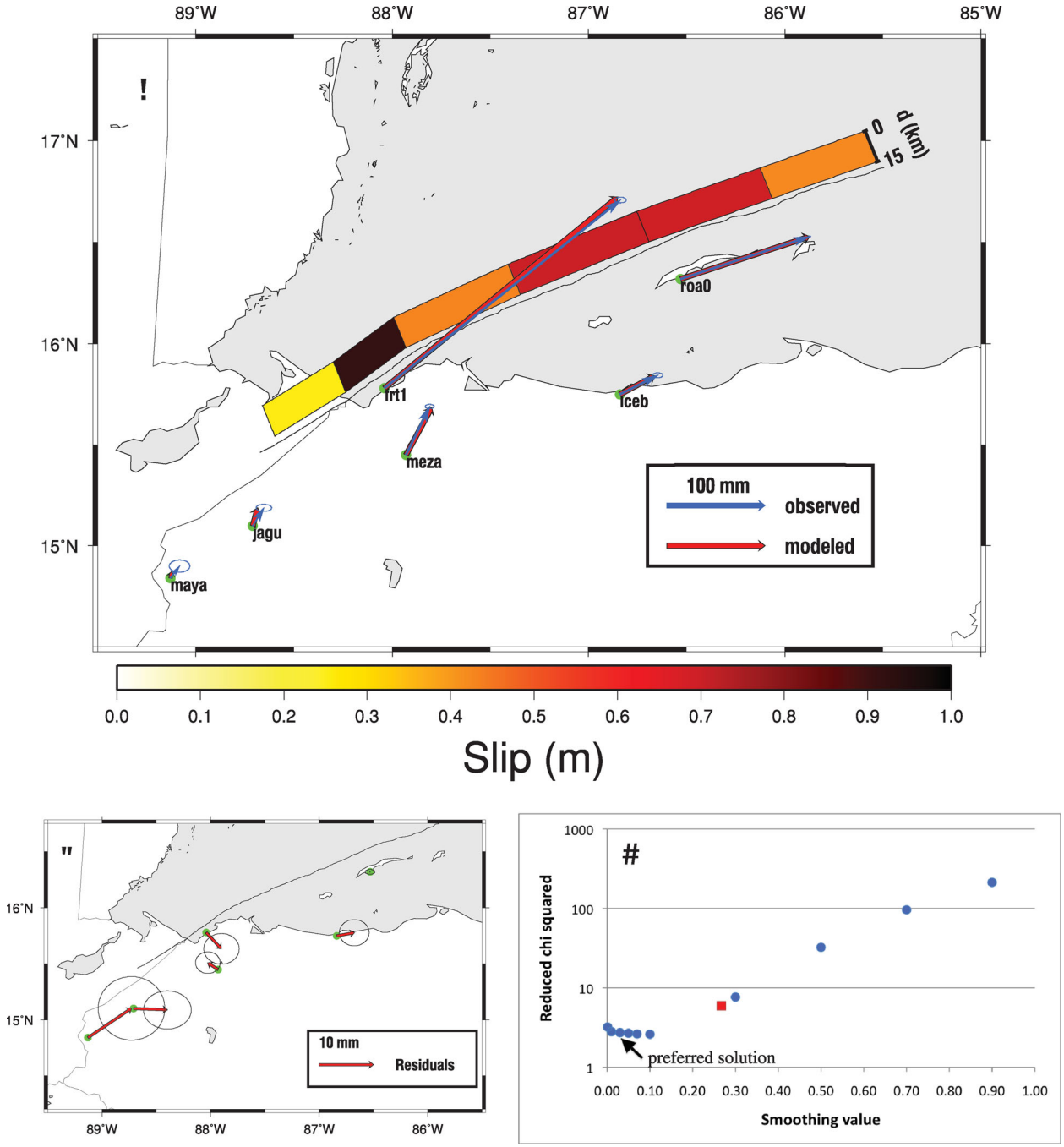

Figure 5. (a) Surface projection of the best-fitting distribution of earthquake slip from inversion of GPS offsets. Blue and red arrows show observed and modelled GPS offsets, respectively. Fault plane is shifted above the fault trace for clarity. (b) Residual coseismic offsets for best-fitting model. (c) Reduced chi-square from inversions of GPS offsets (see text) versus trial values of the smoothing parameter α. Arrow denotes the smoothing parameter for the best-fitting solution ($\alpha = 0.03$). Red square shows location of the L curve smoothing parameter.

SEAMARC II (Rosencrantz & Mann 1991) and the eastern, onshore end of the Motagua fault (Plafker 1976). Moving the assumed fault location several kilometres closer to or farther from the Honduran coast respectively reduces or increases by ∼30 per cent our estimate of ∼0.9 m of coseismic fault-slip along the segment adjacent to GPS site FRT1, but has little effect on the slip estimates for the other segments. The best-fitting seismic slip solution described below independently supports the existence of ∼1 m of slip along this segment of the fault.

3 FAULT-SLIP ESTIMATE FROM TELESEISMIC WAVEFORMS

3.1 Seismic data

We also estimated coseismic slip for the 2009 Swan Islands earthquake from an inversion of broad-band seismic data using a teleseismic body wave inversion program described by Kikuchi & Kanamori (1991, 2003). The seismic slip distribution and source

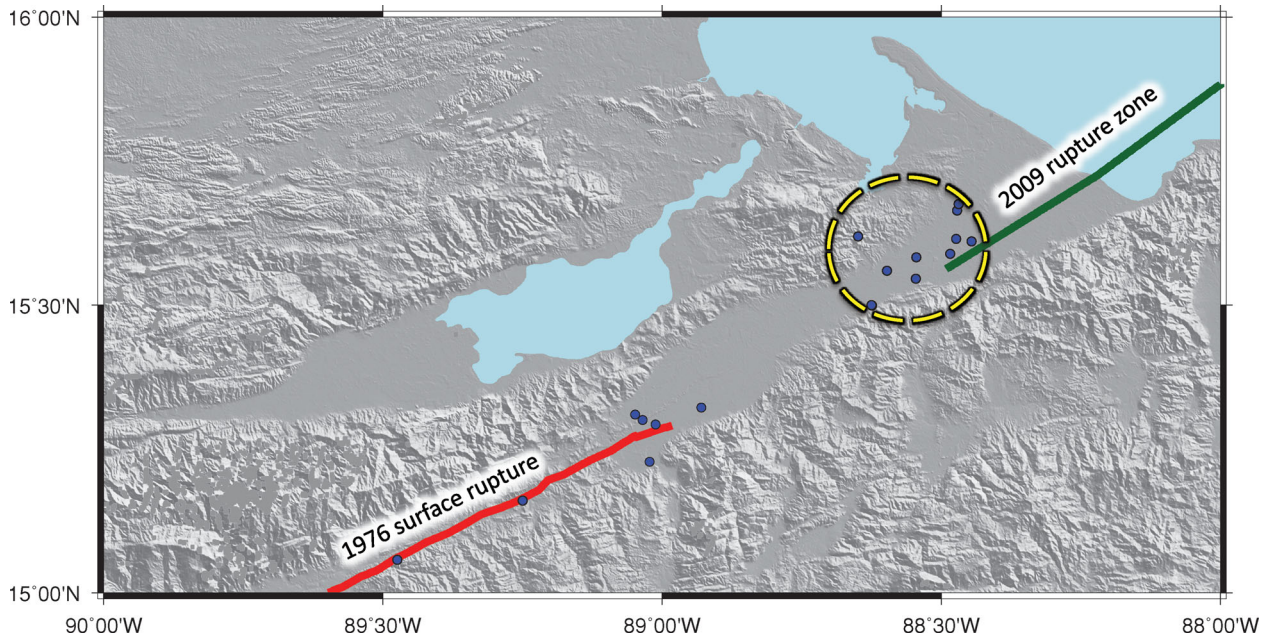

Figure 6. Rupture limits for the $M_s = 7.5$ 1976 Motagua fault earthquake and $M_w = 7.3$ 2009 Swan Islands fault earthquake. Blue circles are aftershocks from the 1976 earthquake from Langer & Bollinger (1979). Yellow ellipse highlights the easternmost aftershocks for the 1976 Motagua fault earthquake and red line shows the easternmost limit of surface rupture mapped for this earthquake (Plafker 1976). Green line shows the estimated western limit of the 2009 May 28 Swan Islands fault earthquake. Digital elevation model of eastern Guatemala and northwestern Honduras is from Space Shuttle Radar Topographic Mission 90 m data.

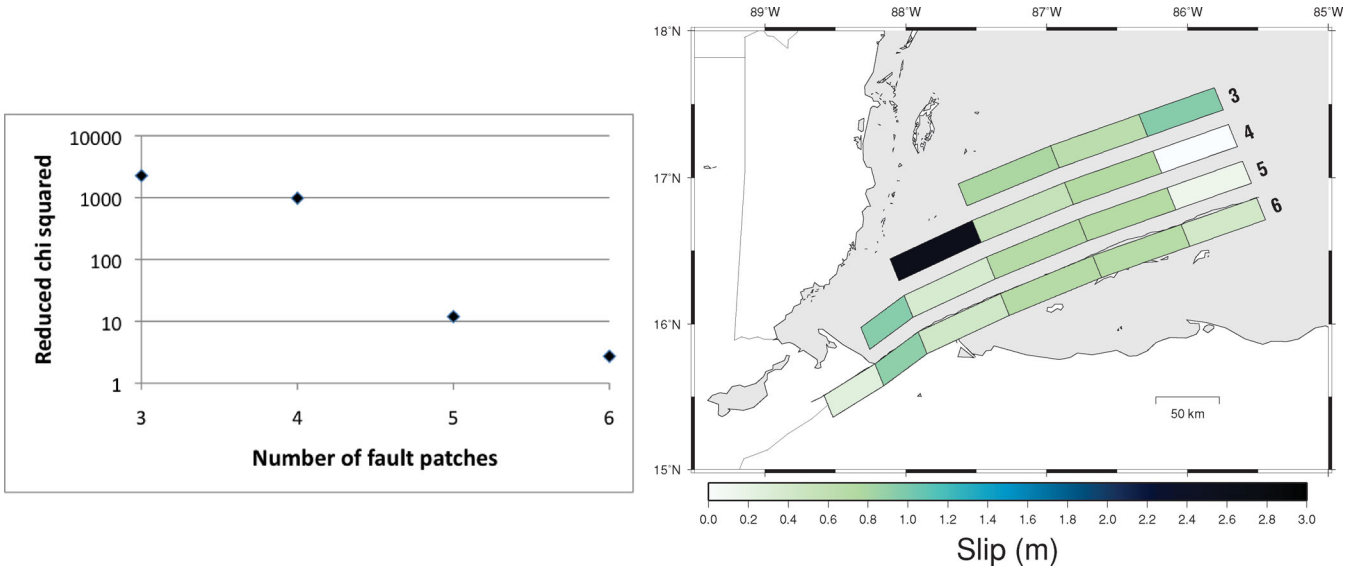

Figure 7. Trade-off between GPS model fit and assumed western limit of the 2009 earthquake rupture zone. (Left) Variation in the fit to the GPS offsets used to estimate the best fault-slip distributions as a function of the number of fault patches assumed in the inversion. Corresponding fault geometries are shown in the right panel. (Right) Estimated fault-slip distributions for three-patch through six-patch fault models. The six-patch fault model follows the trace of the fault; other slip distributions are offset vertically for clarity. Misfit is not significantly reduced until at least five patches are used. The six-patch model is the best-fitting solution from Fig. 5a.

time function, described below, are estimated from Fast Archive Recovery Method (FARM) event broad-band data for 25 stations retrieved from the IRIS Data Management Center, all with high signal-to-noise ratios and located at epicentral distances ranging from 26° to 89° (Fig. 9a). Prior to their inversion, the data were bandpass filtered between 0.01 and 0.12 Hz and the first 80 s following the *P*- and *SH*- wave arrivals were selected.

3.2 Inversion assumptions

The fault plane we use for our seismic slip source modelling extends 15 km down dip, 300 km along strike, and strikes N68°E, consistent with SeaMARC II mapping (Rosencrantz & Mann 1991; Rogers & Mann 2007). Inversions in which we use a fault dip of 68°, the same as for the global CMT catalogue or instead assume a vertical fault

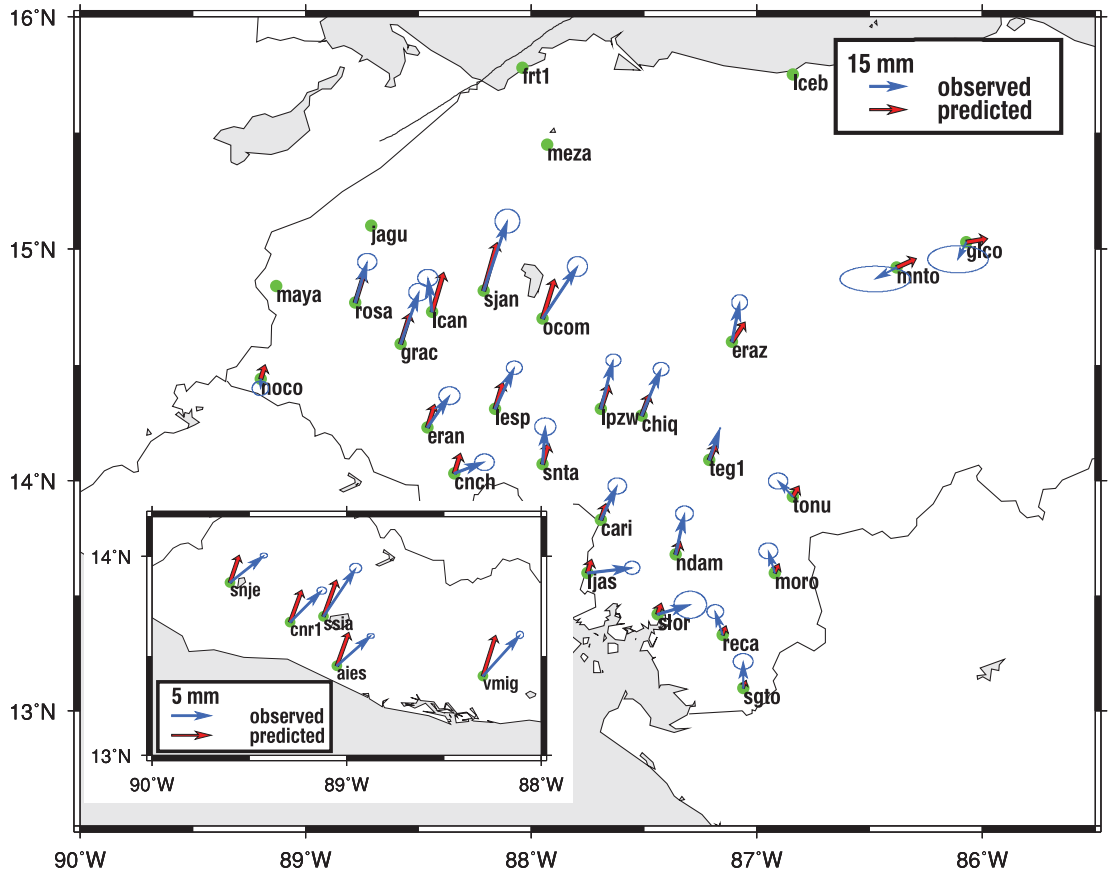

Figure 8. Comparison of measured coseismic offsets (blue) to offsets predicted by the best fitting coseismic slip distribution (red) (Fig. 5) at stations not used to estimate the best-fitting model. Inset shows at a larger scale the predicted and observed offsets at five continuous GPS sites in El Salvador.

dip give slip solutions that differ insignificantly. We thus adopted the 68° dip for consistency with the global CMT catalogue. The moment rate function is described by three or four triangle functions with 8 s duration and 4 s of overlap. The Jeffreys–Bullen velocity model was used in the computation of the body wave Green's functions. *SH* waveforms were downweighted in the inversion to stabilize the solution and keep the predicted seismic moment from reaching unreasonably high values. We explored a range of possible rupture velocities and achieved the best fits for those from 2.8 to 4.0 km s^{-1}.

3.3 Inversion results: seismologically derived fault-slip

Because many combinations of input parameters (e.g. rupture velocity, number of triangle functions, *SH* weighting) produced seismic slip distributions with similar misfit, moment and magnitude, we 'stacked' and averaged the slip distributions of the best-fitting models to amplify their common features and suppress their differences. To determine the range of slip distributions with acceptable fits, we inverted the seismic data many times while varying the parameters described above. From these estimates, we selected 12 models with the lowest misfit, with seismic moments similar to those estimated by the USGS and global CMT and whose input parameters span the plausible range of rupture velocities.

Fig. 9 shows the average slip from the 12 best-fitting models and two end-member slip distributions for comparison. The averaged seismic slip distribution consists of an area of high slip (~1.2 m) just west of Roatan Island and the epicentre, a second area of high slip (~1 m) ~250 km west of the epicentre (offshore from FRT1) and less slip (~0.4 m) between (Fig. 9b). The seismic moment for our stacked seismic slip distribution is 12.6×10^{19} Nm, consistent with both our geodetic estimate of 12.4×10^{19} Nm and moments reported by the USGS and global CMT. The source time function (Figs 9e and f) consists of a long-duration energy release with one larger pulse at 60 s (common to all models) and the rest of the energy relatively evenly distributed over 90 s.

4 COULOMB STRESS CHANGES FROM THE 2009 SWAN ISLANDS FAULT EARTHQUAKE AND ASSOCIATED TRIGGERED EARTHQUAKES

As with any large earthquake, fault-slip alters the local stress field such that nearby faults are driven closer to or further from failure. We therefore calculated the Coulomb stress changes induced by the 2009 May earthquake using our best-fitting geodetic slip distribution as input to Coulomb 3.2 (Lin & Stein 2004; Toda *et al*. 2005). Coulomb Stress changes are calculated with the Coulomb failure criterion: $\Delta\sigma_f = \Delta\tau_s + \mu' \Delta\sigma_n$ where $\Delta\sigma_f$ is the change in failure stress on receiver faults, $\Delta\tau_s$ is the shear stress change, μ' is the fault's effective coefficient of friction and $\Delta\sigma_n$ is the change in normal stress. Material properties assumed for the calculations include a shear modulus G of 40 GPa, Poisson's ratio ν(0.28) and Young's modulus E of 102.4 GPa ($E = 2G(1 + \nu)$). A typical value of 0.4

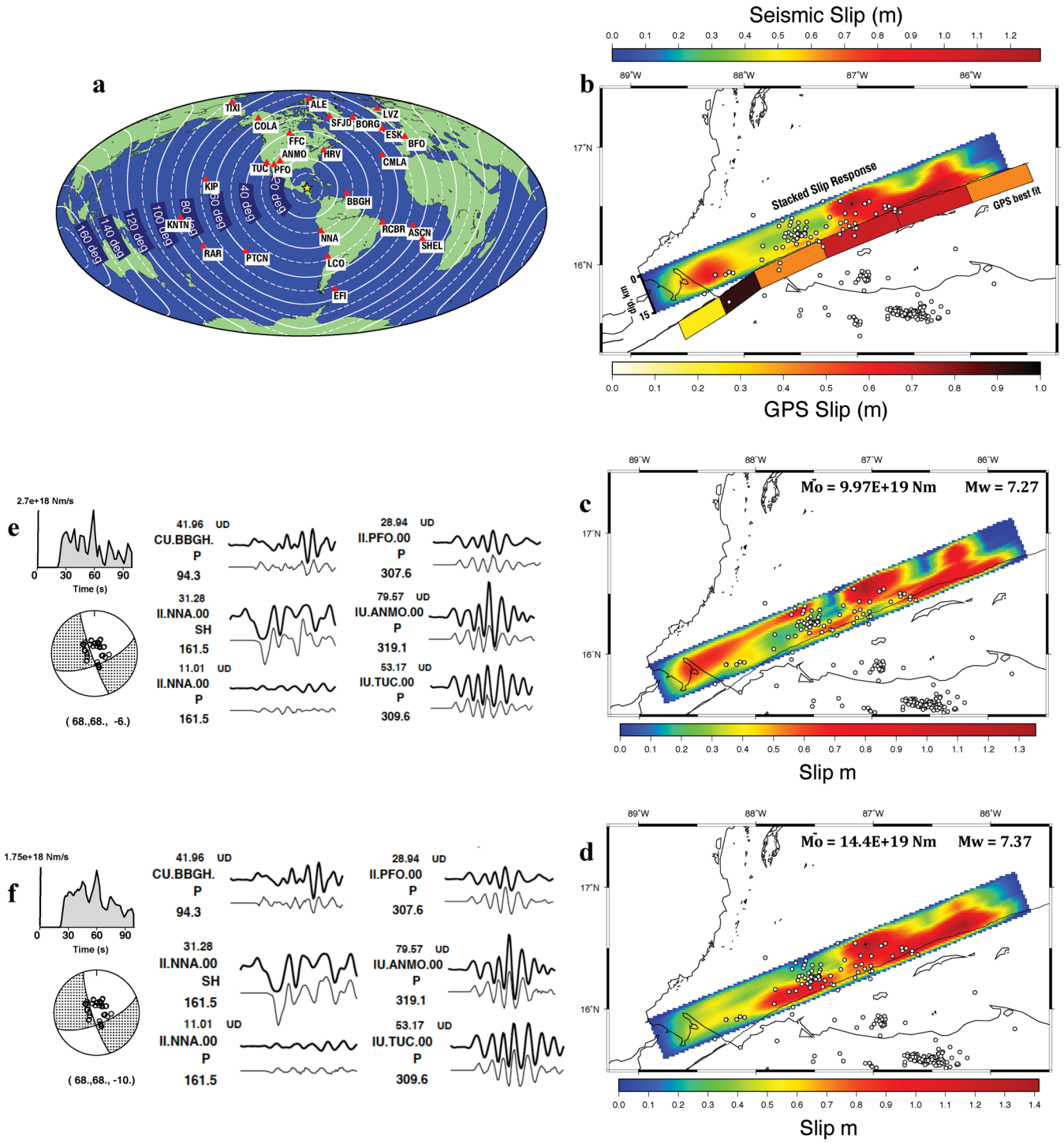

Figure 9. (a) Seismic stations used in the inversion with epicentral distances in white. (b) 'Stacked' average seismic slip response from twelve plausible models. GPS-based best-fitting slip distribution is shown and labelled for comparison. The top of the GPS slip distribution follows the trace of the Swan Islands fault. White circles denote locations of aftershocks recorded by a local seismic array (described in text). (c) and (d) show two representative end member solutions of the 12 seismic-slip models used in the stack. (e) and (f) show their corresponding source time functions, focal mechanisms and fits to subsets of the seismograms used to estimate them. The uppermost waveform in each seismogram is observed and the lowermost waveform is predicted by the seismic model.

is selected for the effective coefficient of fault friction, however our results are relatively insensitive to a range of assumed values ($\mu' = 0.2$–0.8). Positive changes in $\Delta\sigma_f$ are thought to promote failure (King *et al*. 1994), are correlated with aftershock rates (Stein 1999) and may influence where future earthquakes nucleate.

Fig. 10(a) shows the Coulomb stress changes of a maximum of 1 bar at seismogenic depths (10 km) for faults with strikes similar to the Swan Islands fault. As expected, stresses increase both west and east of the rupture limits along strike via enhanced fault-parallel shear stresses. The increased stress at the western end of the rupture

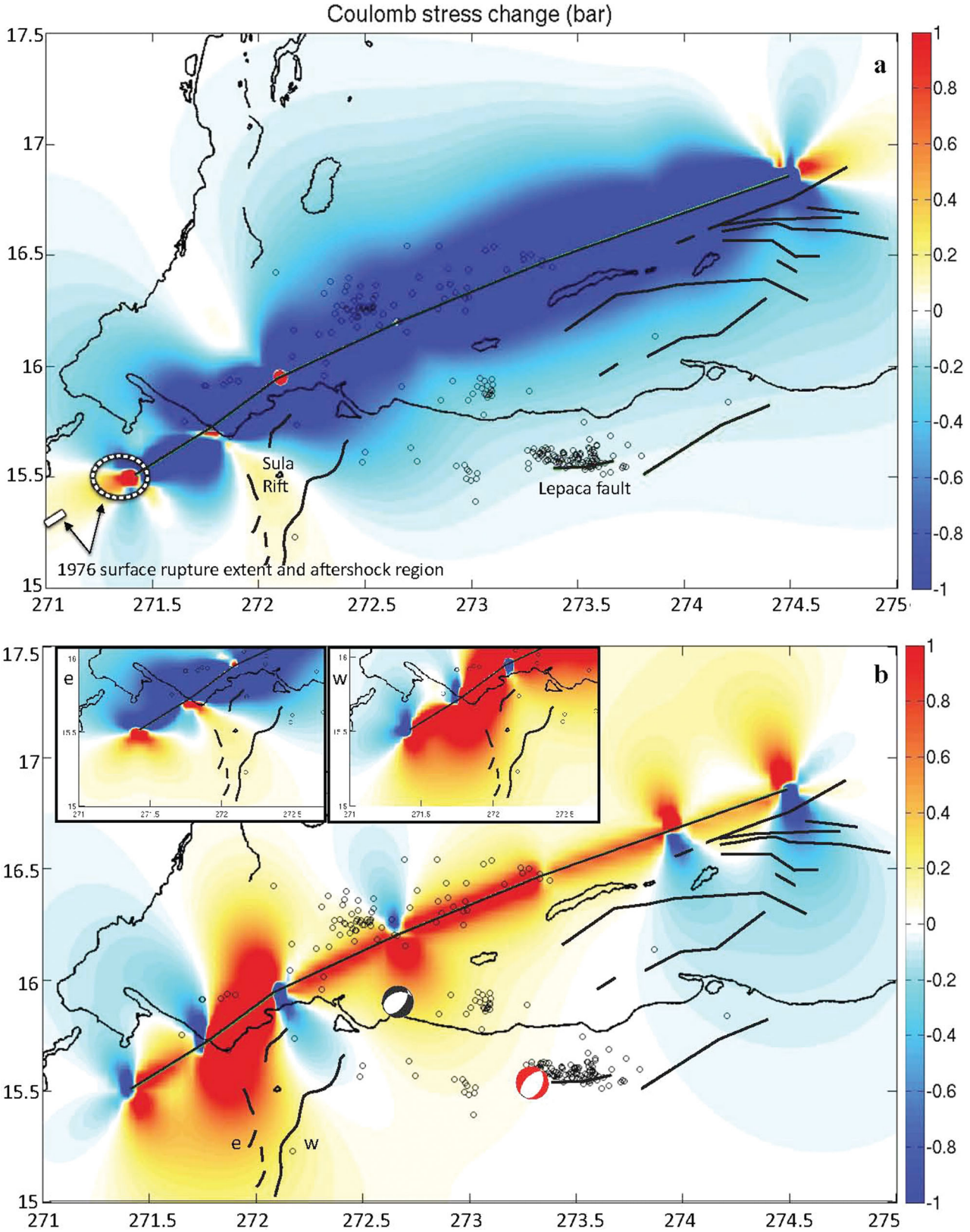

Figure 10. (a) Coulomb stress changes at 10 km depth predicted by best-fitting GPS slip distribution for strike-slip faults with the same orientation as the Swan Islands fault. White line and dashed circle show 1976 surface rupture and aftershock locations, respectively, from Fig. 6. (b) Coulomb stress change (CSC) for known normal faults in northern Honduras and faults located offshore from the best-fitting GPS slip solution for the 2009 Swan Islands fault earthquake. The red and black focal mechanisms are for the $M = 5.1$ 2009 June 2 and $M = 2009$ 5.4 June 8 triggered earthquakes, respectively. Open circles show aftershocks recorded by the regional temporary network described in the text. The two inset maps show the predicted Coulomb stress changes for eastern (e) and western (w) Sula Rift faults. Fault locations taken from Rogers & Mann (2007).

zone loads the eastern end of the Motagua fault almost precisely at the eastern limit of rupture, determined from aftershock distribution, during the $M_s = 7.5$ 1976 earthquake (Fig. 10a).

We also determine the Coulomb stress changes along the ∼N70°E striking normal faults that are located south of the Swan Islands in the Caribbean Sea and northern Honduras (Rogers & Mann 2007). Positive Coulomb stress changes occurred across the normal faults in nearly all the region to the south and west of the rupture zone, thereby making them more prone to failure. In the same region, the June 2 $M = 5.1$ and June 8 $M = 5.4$ normal-faulting earthquakes occurred 5 and 11 d after the 2009 May 28 main shock, respectively (Fig. 10b). The $M = 7.3$ main shock thus appears to have triggered two moderate-sized normal-faulting earthquakes on faults south of the Swan Islands fault. Coulomb stress changes were also calculated for the ∼N10°E normal faults that make up the Sula Rift (inset Fig. 10b). These also indicate a similar likelihood of failure in the event of a Swan Islands fault earthquake. The Coulomb stress calculations and occurrence of these two earthquakes indicate that the region of normal faults in and near northern Honduras is situated in a location where unclamping occurs in response to large strike-slip earthquakes on the Swan Islands fault.

Because the above relationship may be important for earthquake forecasting scenarios and future disaster preparedness for northern Honduras, we also predicted Coulomb stress changes for end-member slip distributions and dipping faults. We found that these alternative fault models did not significantly change the major features of the Coulomb stress pattern. Our above results and any conclusions derived from them thus appear to be robust.

On 2009 June 2, 5 d after the $M = 7.3$ earthquake, a $M = 5.1$ normal-faulting earthquake occurred at the western end of the Lepaca fault, a strike-slip fault in northern Honduras (Fig. 10b). Numerous small earthquakes along a ∼50-km-long, east–west striking segment of the Lepaca fault occurred after the $M = 5.1$ earthquake (Fig. 10b). We considered three explanations for the spatial and temporal locations of these numerous earthquakes, as follows: (1) the earthquakes were triggered in response to the Swan Islands fault main shock, (2) they were aftershocks of the $M = 5.1$ earthquake, presumably along the Lepaca fault and (3) the $M = 5.1$ earthquake ruptured a fault at the western end of the Lepaca fault, which then triggered the sequence of small events along the Lepaca fault.

Several lines of evidence argue against the first two hypotheses. Regarding the first hypothesis, the Coulomb stress changes predicted for the strike-slip Lepaca fault from the $M = 7.3$ Swan Islands earthquake are negative and thus do not promote failure on that fault (Fig. 10a). The seismicity associated with the Lepaca fault thus appears unlikely to have been triggered by the Swan Islands fault main shock. Regarding the second hypothesis, empirical relations between seismic moments and earthquake rupture lengths (Pegler & Das 1996) indicate that the rupture length for a $M = 5.1$ earthquake ($M_o = 6.4 \times 10^{16}$ Nm) should be no more than 10 km long and more likely less than 5 km long, a factor of 5–10 shorter than the observed 50-km-long aftershock zone reported above. This suggests that the earthquakes do not define the rupture plane for the $M = 5.1$ event.

Some evidence supports the third explanation postulated above. The Coulomb stress changes for the 2009 May 29 Swan Islands fault earthquake calculated for one nodal plane of the June 2 $M = 5.1$ earthquake are small and positive near the western end of the Lepaca fault (Fig. 10b). The larger $M = 7.3$ earthquake may thus have unclamped a normal fault at the western end of the Lepaca fault, which in turn triggered the 50-km-long earthquake sequence on the strike-slip Lepaca fault. This may be an example of a cascading series of triggered earthquakes within a system of interacting faults.

5 DISCUSSION

5.1 Role of fault-slip in damage in northern Honduras

Earthquake damage reports compiled by the Honduran government indicate the highest local damage occurred along areas of the north coast (demarcated by the red zones in the Fig. 11 inset), more than 150 km west of the epicentre. In contrast, less damage was reported on the island of Roatan (Shulman & Mooney 2009) despite its proximity to the epicentre. Local geologic conditions were partially responsible for the elevated damage far from the epicentre (Shulman & Mooney 2009); however, both our geodetic and seismic slip solutions indicate that some of the damage was caused by the proximity of these areas to the region of high fault-slip directly offshore from the area of highest damage (Fig. 11).

5.2 Earthquake triggering and seismic hazard: northern Honduras

Rogers & Mann (2007) define a North Coast Province in Honduras, including offshore areas north to the Swan Islands fault, where deformation is dominated by normal and strike-slip faulting. The changes in Coulomb stresses described above indicate that a major earthquake on the Swan Islands fault promotes failure along normal faults in this province. The occurrence of two $M > 5$ normal-faulting earthquakes along separate faults in this province following the 2009 May earthquake is consistent with this triggering relationship. The possible triggering of numerous microseisms along a ∼50-km-long length of the strike-slip Lepaca fault by the $M = 5.1$ 2009 June 2 normal-faulting earthquake indicates that triggered normal-faulting earthquakes may promote failure along the E–W striking strike-slip faults in this province. For these reasons, communities in northern Honduras should be prepared for both future large ($M \sim 7$) Swan Islands fault earthquakes as well as smaller triggered earthquakes in the aftermath of the main shock(s).

5.3 Estimated earthquake recurrence interval for the Swan Islands fault

A maximum of ∼1 m of fault-slip occurred during the 2009 May 28, Swan Islands earthquake. North America–Caribbean Plate motion is predicted to be 19.4 ± 0.4 mm yr^{-1} along this part of the Swan Islands fault (DeMets *et al*. 2010), thereby implying a ∼50-yr recurrence interval between similar-sized earthquakes assuming that other strike-slip earthquakes do not accommodate a significant fraction of the plate motion. Since 1976, the cumulative moment for other strike-slip earthquakes along this segment of Swan Islands fault, 0.29×10^{20} Nm, accounted for 18 per cent of the total slip budget and the 2009 event the remaining ∼82 per cent. The recurrence interval may thus be ∼20 per cent shorter than 50 yr if the 2009 earthquake was characteristic for this segment.

In contrast to the several-decade-long recurrence interval for the Swan Islands fault, estimates of the recurrence interval for large earthquakes on the adjacent Motagua fault range from 160 yr (Plafker 1976) to 180–755 yr (Schwartz *et al*. 1979), as calculated from the maximum slip (3.4 m) during the $M = 7.5$ 1976 February 4 Motagua fault earthquake, and terrace offsets and ages in conjunction with the 1976 earthquake, respectively. Earthquakes

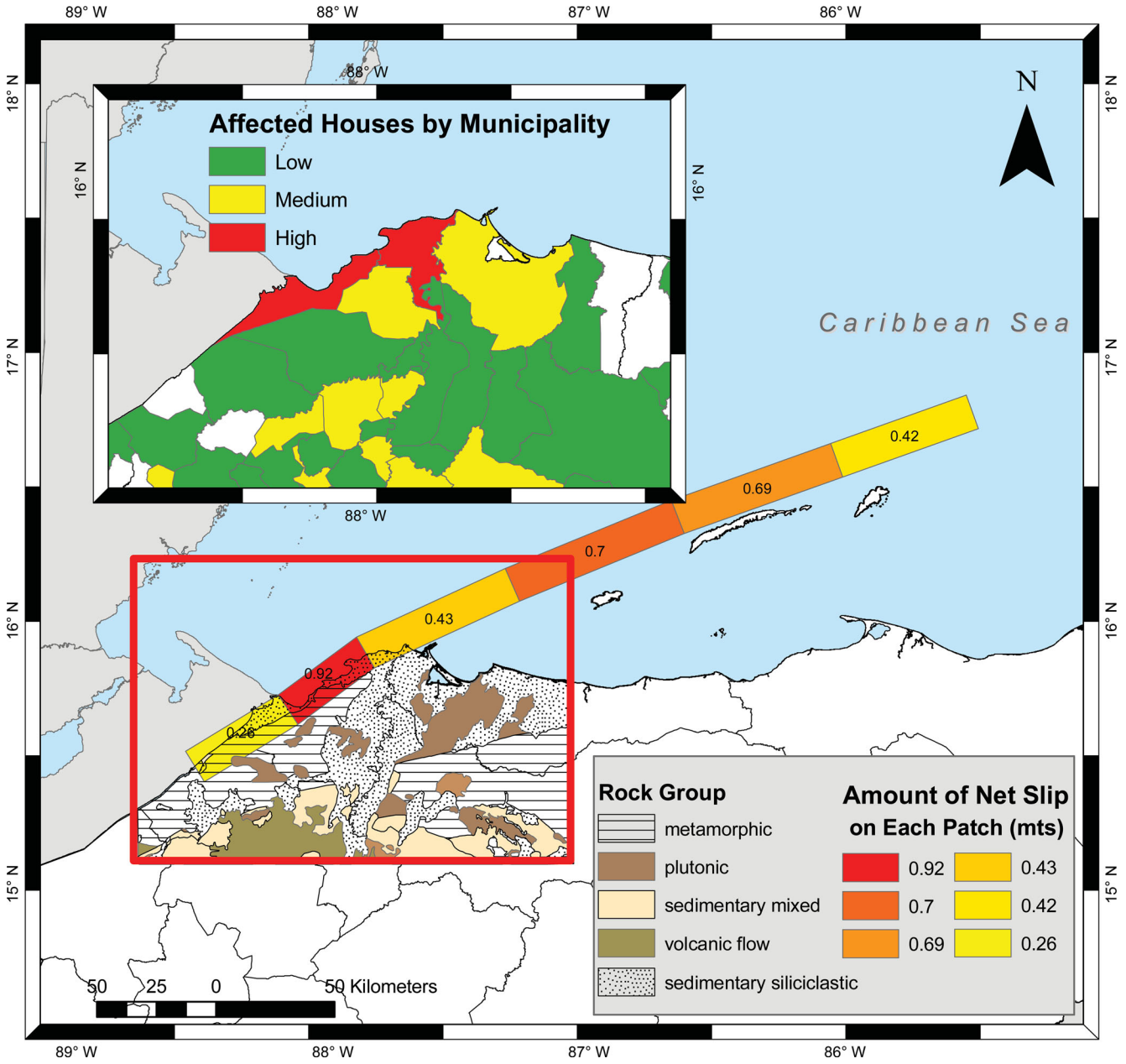

Figure 11. Best-fitting GPS-based fault-slip model for the 2009 Swan Islands fault earthquake with geologic map (within the red rectangular area) and relative numbers of damaged houses by municipality (inset). The region of high fault-slip near the western end of the rupture zone coincides with the region of high damage shown in the inset map, suggesting that the elevated damage was caused by a combination of proximity to the rupture zone and the presence of unconsolidated near-surface sediments (Shulman & Mooney 2009).

along the Swan Islands fault may therefore be smaller and more frequent than for the Motagua fault. A simple comparison of earthquakes along the Motagua fault and western half of the Swan Islands fault since 1976 indirectly supports this conclusion. Since 1976, 10 strike-slip earthquakes with magnitudes greater than 5.5 have ruptured the western half of the Swan Islands fault (Fig. 1). During the same period, no $M > 5.5$ strike-slip earthquakes have ruptured the Motagua fault (Fig. 1). Based on evidence that earthquakes along the Queen Charlotte Islands and San Andreas strike-slip faults increase in magnitude but decrease in frequency with distance from the spreading centres that terminate these faults, Kelleher & Savino (1975) postulate that earthquake size and frequency may depend on lithospheric thickness and heat flow. The contrast between earthquake sizes and recurrence intervals described above for the Swan Islands and Motagua faults supports their hypothesis.

5.4 Role of tectonic setting in the seismicity of the Motagua and Swan Islands fault zones

The different tectonic settings of the Motagua and Swan Islands fault zones may influence their respective earthquakes' size and recurrence interval. The N69°E striking western Swan Islands fault is 6° oblique to the N75°E ± 1° direction of Caribbean–North America Plate motion in this area (DeMets *et al.* 2010), putting the fault under mild transtension. In contrast to the transtensional Swan Islands fault, the arcuate Motagua fault of central and western

Guatemala undergoes an east-to-west transition from transtension to transpression due to a change in the fault's strike and the direction of Caribbean–North America Plate motion (Rodriguez *et al.* 2009). The shorter recurrence interval and smaller magnitudes for ruptures characteristic of the Swan Islands fault in comparison to those for the Motagua fault may be partly or entirely due to the differing stress conditions across these two faults.

6 CONCLUSIONS

Inversions of GPS-recorded coseismic offsets caused by the $M_w = 7.3$ 2009 May 28 Swan Islands fault earthquake and of seismograms from 25 stations at teleseismic distances indicate that coseismic fault-slip averaged ∼0.6 m over a ∼300-km-long length of the Swan Islands fault and extended west to the approximate eastern limit of the 1976 $M = 7.5$ Motagua fault earthquake. Similarities between the independent geodetic and seismologic coseismic slip estimates reinforce the occurrence of high slip (∼1 m) at the western rupture limit, where high levels of damage were reported onshore from the underwater fault. Modelling of the Coulomb stress change due to the earthquake indicates a maximum of 1 bar increase in the failure stress along the eastern end of the Motagua fault, equivalent to ∼8 yr of secular stressing. This represents only a modest advance in the estimated 160-yr-long (Plafker 1976) or 180–755-yr-long (Schwartz *et al.* 1979) earthquake cycle of the Motagua fault. Two $M > 5$ normal-faulting earthquakes within 11 d of the main shock suggest there is a triggering relationship between large earthquakes on the Swan Islands fault and normal-faulting in and offshore from northern Honduras. Coulomb stress modelling supports this conclusion.

ACKNOWLEDGMENTS

This work was funded by NSF grant EAR-0538131 (DeMets). We thank Universidad Nacional Autonoma de Honduras and Servicio Nacional de Estudious Territoriales of El Salvador for logistical support. We also thank UW technician Neal Lord for his dedicated work in the field. We thank Helene Lyon-Caen and Paul Mann for their insightful reviews that led to an improved paper. Data critical for this work were procured from the Incorporated Research Institutions for Seismology (IRIS) WILBER II database. Some of this material is based on data provided by the UNAVCO Facility with support from the National Science Foundation (NSF) and National Aeronautics and Space Administration (NASA) under NSF Cooperative Agreement No. EAR-0735156. Figures were produced using Generic Mapping Tools software (Wessel & Smith 1991).

REFERENCES

Altamimi, Z., Collilieux, X. & Metivier, L., 2011. ITRF2008: an improved solution of the international terrestrial reference frame, *J. Geodyn.,* **85,** 457–473.

Alvarez-Gomez, J.A., Meijer, P.T., MartÌnez-DÌaz, J.J. & Capote, R., 2008. Constraints from finite element modeling on the active tectonics of northern Central America and the Middle America Trench, *Tectonics,* **27,** TC1008, doi:10.1029/2007TC002162.

Correa-Mora, F., DeMets, C., Cabral-Cano, E., Marquez-Azua, B. & Diaz-Molina, O., 2008. Interplate coupling and transient slip along the subduction interface beneath Oaxaca, Mexico, *Geophys. J. Int.,* **175,** 269–290.

DeMets, C., Gordon, R.G. & Argus, D.F., 2010. Geologically current plate motions, *Geophys. J. Int.,* **181,** 1–80.

Guzman-Speziale, M., 2001. Active seismic deformation in the grabens of northern Central America and its relationship to the relative motion of the North America–Caribbean plate boundary, *Tectonophysics,* **337,** 39–51.

Guzman-Speziale, M., Pennington, W.D. & Matumoto, T., 1989. The Triple junction of the North America, Cocos, and Caribbean Plates: seismicity and tectonics, *Tectonics,* **8,** 981–997.

Hansen, P.C., 1992. Analysis of discrete ill-posed problems by means of the L-curve, *SIAM Rev.,* **34,** 561–580.

Kelleher, J. & Savino, J., 1975. Distribution of seismicity before large strike slip and thrust-type earthquakes, *J. geophys. Res.,* **80,** 260–271.

Kikuchi, M. & Kanamori, H., 1991. Inversion of complex body waves–III, *Bull. seism.l Soc. Am.,* **81,** 2335–2350.

Kikuchi, M. & Kanamori, H., 2003. Note on Teleseismic Body-Wave Inversion Program. Available at: http://www.eri.u-tokyo.ac.jp/ETAL/KIKUCHI/ (last accessed 2011 May 25).

King, G.C.P., Stein, R.S. & Lin, J., 1994. Static stress changes and the triggering of earthquakes, *Bull. seism. Soc. Am.,* **84,** 935–953.

Langer, C.J. & Bollinger, G.A., 1979. Secondary faulting near the terminus of a seismogenic strike-slip fault: Aftershocks of the 1976 Guatemala earthquake, *Bull. seism. Soc. Am.,* **69,** 427–444.

Larsen, S.C., 1992. Displacement modeling of dislocations, *PhD thesis*, California Institute of Technology, Pasadena, CA.

Lawson, C.L. & Hanson, R.J., 1974. *Solving Least Squares Problems,* Prentice-Hall, Englewood Cliffs, NJ.

Lin, J. & Stein, R.S., 2004. Stress triggering in thrust and subduction earthquakes and stress interaction between the southern San Andreas and nearby thrust and strike-slip faults, *J. geophys. Res.,* **109,** B02303, doi:10.1029/2003JB002607.

Lyon-Caen, H. *et al*., 2006. Kinematics of the North American-Caribbean-Cocos plates in Central America from new GPS measurements across the Polochic-Motagua fault system, *Geophys. Res. Lett.,* **33,** L19309, doi:10.1029/2006GL027694.

Mann, P., Tyburski, S.A. & Rosencrantz, E., 1991. Neogene development of the Swan Islands restraining-bend complex, Caribbean Sea, *Geology,* **19,** 823–826.

Marquez-Azua, B. & DeMets, C., 2003. Crustal velocity field of Mexico from continuous GPS measurements, 1993 to June 2001: implications for the neotectonics of Mexico, *J. geophys. Res.,* **108,** 2450, doi:10.1029/2002JB002241.

Pegler, G. & Das, S., 1996. Analysis of the relationship between seismic moment and fault length for large crustal strike-slip earthquakes between 1977–92, *Geophys. Res. Lett.,* **23,** 905–908.

Plafker, G., 1976. Tectonic aspects of the Guatemala Earthquake of 4 February 1976, *Science,* **193,** 1201–1208.

Rodriguez, M., DeMets, C., Rogers, R., Tenorio, C. & Hernandez, D., 2009. A GPS and modelling study of deformation in northern Central America, *Geophys.l J. Int.,* **178,** 1733–1754.

Rogers, R.D. & Mann, P., 2007. Transtensional deformation of the western Caribbean-North America plate boundary zone, *Geol. Soc. Am. Spec. Pap.,* **428,** 37–64.

Rosencrantz, E. & Mann, P., 1991. SeaMARC II mapping of transform faults in the Cayman Trough, Caribbean Sea, *Geology,* **19,** 690–693.

Schwartz, D.P., Cluff, L.S. & Donnelly, T.W., 1979. Quaternary faulting along the Caribbean-North American plate boundary in Central America, *Tectonophysics,* **52,** 431–445.

Shulman, D.J. & Mooney, W.D., 2009. Site survey of May 28, 2009 Honduran earthquake, *Geol. Soc. Am., Abstr. Prog.,* **41,** 372.

Stein, R.S., 1999. The role of stress transfer in earthquake occurrence, *Nature,* **402,** 605–609.

Toda, S., Stein, R.S., Richards-Dinger, K. & Bozkurt, S.B., 2005. Forecasting the evolution of seismicity in southern California: Animations built on earthquake stress transfer, *J. geophys. Res.,* **110,** B05S16, doi:10.1029/2004JB003415.

Wessel, P. & Smith, W.H.F., 1991. Free software helps map and display data, *EOS, Trans. Am. geophys. Un.,* **72,** 455–473.

White, R.A., 1985. The Guatemala earthquake of 1816 on the Chixoy-Polochic fault, *Bul. seism. Soc. Am.,* **75,** 455–473.

Zumberge, J.F., Heflin, M.B., Jefferson, D.C., Watkins, M.M. & Webb, F.H., 1997. Precise point positioning for the efficient and robust analysis of GPS data from large networks, *J. geophys. Res.,* **102,** 5005–5017.